

Szilard Engines as Quantum Thermodynamical Systems

Maryam Ashrafi,^{*} Fabio Anza,[†] and James P. Crutchfield[‡]

*Complexity Sciences Center and Physics Department,
University of California at Davis, One Shields Avenue, Davis, CA 95616*

(Dated: December 22, 2024)

We discuss the Szilard engine whose working fluid consists of a single quantum-mechanical particle. Following Szilard's original solution of Maxwell's Second Law paradox, which turned on physically instantiating the demon (control subsystem), the quantum engine's design parallels the classically-chaotic Szilard Map that operates a thermodynamic cycle of measurement, thermal-energy extraction, and memory reset. We analyze in detail the dynamical mechanisms by which the quantum engine operates, both its thermodynamic costs and the required information processing to observe and control the particle, comparing these in the quantum, semiclassical, and classical limits. We establish Landauer Principles for information-processing-induced thermodynamic dissipation in the quantum and semiclassical regimes.

Keywords: Landauer Principle, heat engine, information engine, Maxwell Demon

Sparked by Maxwell's infamous thought experiment on the limitations of the Second Law of thermodynamics [1], modern efforts to improve our understanding of thermodynamics at the nanoscale have clearly highlighted information as a thermodynamic resource [2–4]. Starting with Szilard's insights [5], then going through later work by Landauer [6], Bennett [7], and many others [8], the modern developments of stochastic [9] and information thermodynamics [10] allows us to understand Maxwell's demon as an *information engine* [11, 12]—a physical system whose dynamical evolution simultaneously stores and processes information in the service of thermodynamic transformations.

While originally formulated in the classical domain, the inherent microscopic character of these analyses, together with the dramatic improvements in our ability to manipulate systems at the nanoscale, forces us to re-examine these engines to account for quantum behavior. Indeed, descriptions of the quantum version of Szilard's engine have been widely discussed [13–28] and also experimentally realized [29–35].

While a fully accurate description of engine operation requires accounting for the details of the underlying dynamics, the following focuses on two aspects of the quantum Szilard engine. First, we give a more accurate quantum treatment of the demon. Second, we improve on the description of the costs arising in the quantum engine's functionally-distinct stages of its thermodynamic cycle. This involves detailing their dependence on the physical parameters at play, both of system and of the demon.

To do so, we parallel the classical dynamical analysis performed in Ref. [11] that highlighted an interesting

interplay between the entropic cost of erasure and measurement and how they depend on both the parameters of the system and the demon. The results reveal a plethora of interesting phenomena in which the entropic costs of measurement, erasure, and control can be traded-off, while still respecting Landauer's Principle [36]. This achieves a more accurate description of thermodynamic costs that go beyond Landauer's Principle. Moreover, to provide a comprehensive picture, these costs are analyzed in detail in three relevant regimes—quantum, semi-classical, and classical.

Engine Design. The Quantum Szilard Engine (QSE) is an ideal system with which to examine the role of information processing when doing thermodynamic bookkeeping. The engine consists of two components: the System Under Study (SUS) (quantum particle in a box) and a quantum controller or demon. Together, they are surrounded by an incoherent environment that is modeled as a heat bath. The bath keeps everything at thermal equilibrium with inverse temperature β . Paralleling the classical engine's thermodynamic cycle, the QSE goes through a cycle comprising four functionally-distinct operations: *insertion*, *measurement*, *control*, and *erasure*.

At the quantum level, the practical aspects of measurement are nontrivial, thus a more detailed description is necessary than for the classical engine. As noted above, a wide diversity of physical models have been proposed. Here, following Ref. [11] we model the joint system SUS + demon as a single quantum particle but in a $2D$ box of square geometry, with sides of length $\ell = 1$. The horizontal axis, $x \in [0, 1]$, represents the SUS's quantum states, while the vertical axis, $y \in [0, 1]$, represents the demon's microscopic states.

In the first stage of the engine's cycle a barrier is inserted at $x = \delta$ and a coarse-grained projective measurement is performed on the position of the particle, revealing

^{*} ma.ashrafi91@gmail.com

[†] fanza@ucdavis.edu

[‡] chaos@ucdavis.edu

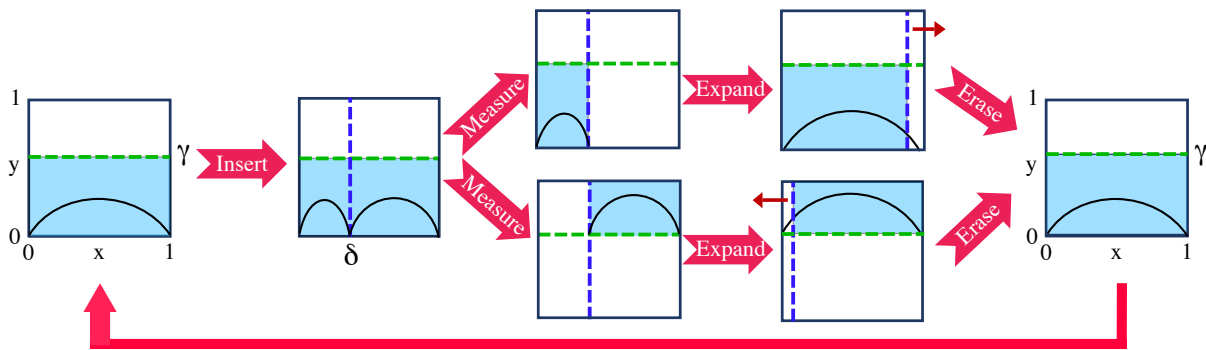


FIG. 1. Quantum Szilard engine thermodynamic cycle: Insert partition, measure particle location, expand single-particle gas, and erase memory of particle location to reset system state for next cycle. Cf. actions of the classical engine under control of the Szilard Map in Fig. 1 of Ref. [11].

whether it is in the left (L) of right (R) side of the barrier. To track the measurement outcome, and correctly operate the subsequent stages, two relevant informational demon states are identified: A with the lower part $y \leq \gamma$ and B with the upper part $y > \gamma$ of the box. The result is that the unit square is partitioned in four macrostates: $\{AL, BL, AR, BR\}$, where $\{L \sim x \in (0, \delta), R \sim x \in (\delta, 1)\}$ and $\{A \sim y \in (0, \gamma), B \sim y \in (\gamma, 1)\}$. We use superscripts to denote the various informational states.

After insertion and measurement, the barrier is released and free to move, such that the particle expands the volume it inhabits, and the reset operation is performed. Since the demon starts in memory state A , if the particle is found on the partition's left, the demon does nothing. If the particle is found on the right side, the demon is in state B and it must reset its state to A . In terms of the informational states of the joint system this action is described by a C-NOT gate [37], correlating the left/right measurement outcome with the the upper/lower informational state of the demon:

$$\begin{aligned} A \otimes L &\rightarrow A \otimes L, & B \otimes L &\rightarrow B \otimes L, \\ A \otimes R &\rightarrow B \otimes R, & B \otimes R &\rightarrow A \otimes R. \end{aligned}$$

Figure 1 gives a visual representation of the overall thermodynamic cycle and the informational states of the joint SUS + demon system. There are two relevant features to call out here. First, the system and demon operate as a joint quantum system. Second, the latter controls the barrier's position and γ controls the demon's informational states. With this setup, the thermodynamic analysis can be carried out, allowing us to explore the interplay between the thermodynamic costs of the various cycle stages as a function of δ and γ . (Details are found in Ref. [38].)

Thermodynamic Regimes. We carried out a detailed thermodynamic analysis, exploring three different phys-

ical regimes. For a quantum particle in a 1D box of length l , the energy levels are $E_n = n^2 \pi^2 \hbar^2 / 2ml^2$ and the partition function $Z = \sum_n e^{-\beta E_n}$ can be written in terms of the Jacobi function: $Z = \frac{1}{2} (\theta_3(0, q) - 1)$, where $\theta_3(0, q) = \sum_{n=-\infty}^{\infty} q^{n^2}$. Here, $q = \exp -\pi (\lambda_d / 2l)^2$ and $\lambda_d = \sqrt{2\pi \hbar^2 / mk_B T}$ is the thermal de Broglie wavelength. $q \in [0, 1]$ implicitly determines the system's quantum nature.

With this, we identify the physical regimes as follows:

- Classical: $\lambda_d \ll \ell$ with partition function $Z^C = \frac{1}{2} \sqrt{\pi / |\ln q|}$.
- Semiclassical: $\lambda_d \leq \ell$ with partition function $Z^S = \frac{1}{2} (\sqrt{\pi / |\ln q|} - 1)$
- Quantum: $\lambda_d > \ell$ where we must use the exact form $Z^Q = (\theta_3(0, q) - 1) / 2$.

At each stage, the systems is in a Gibbs' canonical state. Thus, internal energy and entropy are evaluated by $U = \text{Tr } H \rho = -\partial \log Z / \partial \beta$ and $S = -k_B \text{Tr } \rho \log \rho = k_B \left(1 - \beta \frac{\partial}{\partial \beta}\right) \ln Z$. Figure 2 provides visual confirmation of the difference between the three physical regimes. For the case at hand, in which the box has sides of length $\ell = 1$, we identified the following regimes, parametrized by q or, equivalently, by λ_d : quantum regime is identified with $q \in [0, 0.2]$ or $\lambda_d > 1.4$; semiclassical $\lambda_d \in [0.1, 1.4]$, and classical $\lambda_d < 0.1$.

Engine Initialization. The QSE is prepared in a reference state where the demon (controller subsystem) is in a thermal state localized to the lower part of the box—demon macrostate A —while the SUS is in a thermal state with support on $x \in [0, 1]$. For conciseness, let $Z_{x/y}(\delta/\gamma)$ be the partition function for the SUS + demon joint system when the length of one side of box is δ/γ . Then, analogously, we have the Gibbs canonical state

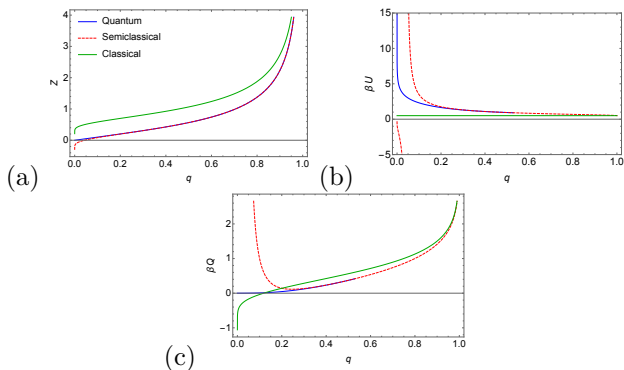


FIG. 2. Distinct thermodynamics of the three physical regimes for a quantum particle in a 1D box: (a) Partition function Z , (b) internal energy βU , and (c) heat βQ versus q in the quantum (blue line), semiclassical (red dashed line), and classical (green solid line) regimes. The clear differences exhibited by these quantities underlie the need to perform the analysis in three different regimes: quantum, semi-classical, and classical. The regimes' boundaries are determined based on these results.

denoted $\rho_{x/y}(\delta/\gamma)$. Then, the macrostate A reference state is $\rho^{(0)} = \rho_x(1) \otimes \rho_y(\gamma)$ with partition function $Z^{(0)} = Z_x(1)Z_y^A(\gamma)$.

Insertion. Perhaps the most distinctive step in the quantum engine cycle comes with the barrier's isothermal insertion. To model insertion we adopt Refs. [39, 40]'s treatment. While Ref. [38] gives details, the essential result can be stated quite simply. The barrier is described by a very thin δ -function potential $V(t) = \lambda(t)\delta(x-\delta)$. As $\lambda(t) \rightarrow \infty$, barrier insertion erases all coherence between the particle on either side. This occurs for all energy eigenstates, thus the same loss of coherence holds for canonical states. This is a key observation. Suppressing off-diagonal matrix elements does not occur due to the subsequent projective measurement of particle position. Thus, this step modifies the thermodynamic cost of measurement and insertion, while leaving unaltered the cost of both. We note that, based on a completely different argument, Ref. [14] also draws this same conclusion.

This implies that the energy cost due to destroying coherences should not be associated with the measurement, but with the insertion process. This thermodynamics differs markedly from the classical case in which insertion has no cost. That said, it is quite interesting to note that the net result renders the SUS + demon joint state a classical superposition between left and right positions *before measurement*. In this way, the semiclassical and classical limits recover the classical result of no thermodynamic cost for insertion.

Reference [38] derives expressions for the changes in entropy, internal energy, and the work done by the system in the three physical regimes. Here, we call out several results summarized in Fig. 3. We compared the thermo-

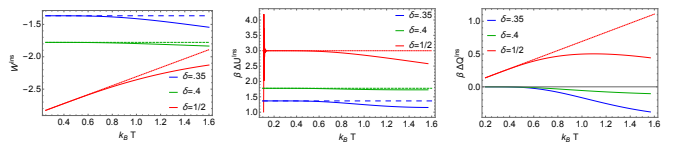


FIG. 3. Thermodynamic cost of insertion at partition locations $\delta \in \{0.35, 0.4, 0.5\}$: Temperature dependence of work W^{ins} , internal energy $\beta\delta U^{\text{ins}}$, and the heat transfer βQ^{ins} in the very low temperature limit where only the ground state is populated (dashed line) and the correct quantum regime (solid line). Appreciable differences between dashed and solid lines, due to higher energy eigenstates, can be seen for very low temperatures. This invalidates using the ground state to model low-temperature behavior.

dynamic costs in the case (i) in which only the ground state is populated, as is usually done for very low temperature (dashed lines) with (ii) the full quantum regime (solid lines). This illustrates how increasing the temperature populates additional energy levels. From this, one appreciates how the barrier position δ directly affects thermodynamic costs of insertion.

Note, for example, how populating additional energy levels results in a generic lowering of all thermodynamic costs. Moreover, one can see how thermodynamic costs deviate significantly from the standard case of $\delta = 0.5$, even for deviations as small as $\delta = 0.4$.

Measurement as Induced Correlation. The second (measurement) stage of the quantum engine's cycle comes in two steps. First, it implements a coarse-grained projective measurement of the particle position, whether it is on the barrier's left or right. Second, it then implements a C-NOT gate that correlates the measurement result (left/right) with the demon's macrostate (A/B). If the particle is found on the left, the demon does nothing, as it was already initialized to the A macrostate. Otherwise, it changes macrostate from A to B .

Appropriate thermodynamic bookkeeping reveals the following average changes in internal energy, entropy, and work. The values are computed averaging over the probability distribution ($p_L(\delta), p_R(1-\delta)$) of finding the particle on the barrier's left or right side, where $p_L(\delta) = Z_x(\delta)/(Z_x(\delta) + Z_x(1-\delta))$ and $p_R(1-\delta) = 1 - p_L(\delta)$. Figure 4 demonstrates that using the classical approximation has a qualitative impact on thermodynamic accounting as the functional dependence on the system parameters, such as temperature, is strongly affected at low temperatures. Moreover, the protocol's specific properties affect the thermodynamic bookkeeping in a nontrivial way. For example, assuming symmetric barrier insertion, $\delta = 1/2$, implies a nonsensitivity to the quantum regime that is lost even for small changes, e.g., $\delta = 1/3$. The existence of this and other nontrivial interplay between the system's

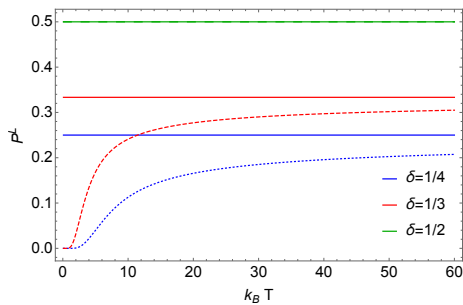


FIG. 4. Temperature dependence of the probability of finding the particle on the left side versus insertion positions $\delta \in \{1/4, 1/3, 1/2\}$. Dashed lines give the quantum probability and solid lines, classical. Here there are two aspects worth noting. First, specific properties of the protocol affect the thermodynamic bookkeeping in a nontrivial way, confirming the need for a more detailed analysis. Second, the validity of the classical assumption is clearly affected by the interplay between the system's parameter δ and the temperature.

parameters and the temperature confirms the need of such detailed analysis.

Figure 5 shows how changes in internal energy, entropy, and work depend on the system parameter δ and demon parameter γ . (The sequel Ref. [38] details the calculations.) Here, we note that at $\gamma = 0.5$, where the informational states of the demon are symmetric, there is no work or energy cost associated with the measurement. However, including the demon and its quantum nature in the model allows to look beyond the $\gamma = 0.5$ line; for example, to account for experimental uncertainties. We can see how this markedly changes the thermodynamics of the measurement step, resulting in nonzero contributions for both the energetic and work cost. Furthermore, one can appreciate how the symmetry $\delta \rightarrow 1 - \delta$, that one naively expects to hold, is present if and only if the demon's informational states are truly equivalent ($\gamma = 0.5$). It does not hold at $\gamma \neq 0.5$.

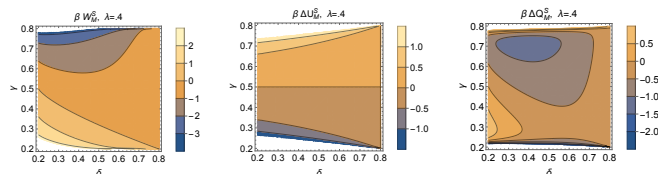


FIG. 5. Barrier partition δ and demon memory γ dependence of thermodynamic costs during measurement and correlation steps: Work βW_M^S , internal energy $\beta \Delta U_M^S$ and entropy $\beta \Delta Q_M^S$ as a function of δ and γ at $\lambda_D = 0.4$.

Control. After measurement and contingent on the resulting demon-memory macrostate, the particle pushes on the barrier isothermally to move it left or right, thereby extracting work $-\sum_n P_n dE_n$ from the ambient heat bath. Figure 6 shows how the energy, entropy, and work func-

tionally depend on δ and γ . Again, Ref. [38] derives the analytical expressions. The thermodynamic costs of the control stage are completely independent of the details of the demon's informational states, while still exhibiting interesting dependence on temperature and δ . Figure 6 plots the thermodynamic cost as a function of δ and λ_D , which stands in for the temperature dependence. There, we see how the classical result is approached at high temperature. This stage reveals more obvious features, too: both the extracted work and the entropic cost monotonically decrease as $|\delta - 0.5|$ increases, while the internal energy change depends only on the temperature.

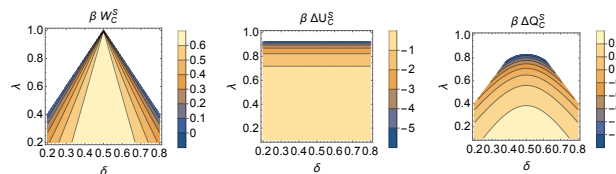


FIG. 6. Thermodynamic resources—work, internal energy, and entropy—of thermal energy extraction during the control stage as a function of λ_D and δ . The symmetry of the box with respect to $\delta = 0.5$ is reflected in the costs. All quantities monotonically decrease with λ_D . While the internal energy change does not depend on δ , both the extracted work and decrease monotonically as we move away from the symmetric configuration $\delta = 0.5$.

Erasure. Finally, we come to the last stage of the engine cycle: Erasure. This reset to the initial overall system state enforces the engine's operating in a thermodynamic cycle. Landauer's original claim was that all thermodynamic cost arose from such erasure and not measurement [36].

Figure 7 shows how ΔU , ΔS , and W depend on δ and γ , revealing interesting nonmonotonic behavior in the dissipated heat. (As with other stages, analytical expressions are available in the sequel Ref. [38].) Again, this is explained in terms of the breaking $\delta \rightarrow 1 - \delta$ symmetry, which is present only on the line $\gamma = 0.5$. This behavior reveals that analyses with this symmetry lack an essential element: A quantum description of the demon. Implicitly, this is equivalent to the assumption that the demon's informational states are essentially equivalent and so neglect, for example, experimental uncertainties or structural imperfections.

This interpretation is also confirmed in Fig. 8, which shows how the work cost to perform erasure vanishes only when the demon informational states have such symmetry—viz., $\gamma = 1 - \gamma = 1/2$. Otherwise, if $\gamma \neq 1/2$, perhaps due to implementation inaccuracies, there is a nonzero work-cost to account for, whose value depends on both γ and δ .

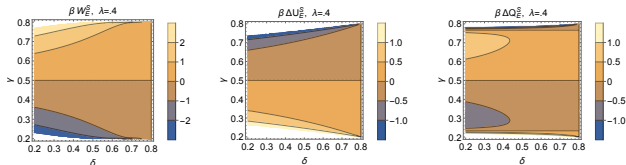


FIG. 7. Thermodynamic costs during erasure: Work, internal energy, and dissipated heat as a function of δ and γ at $\lambda_D = 0.4$. The nonmonotonic behavior of $\beta \Delta Q_E^E$ in $|\delta - 0.5|$ is caused by the lack of symmetry between the informational states at $\gamma \neq 1/2$.

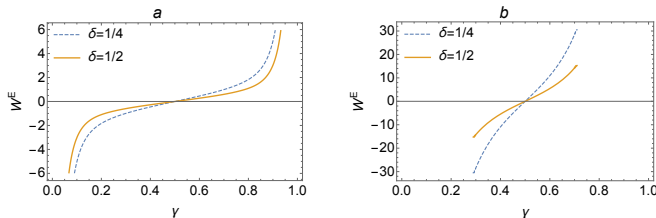


FIG. 8. Erasure work W^E as a function of demon macrostate A size (γ) for (a) $\lambda_D = 1/4$ and (b) $\lambda_D = 2$.

Discussion and final remarks. Extending a recent dynamical analysis [11] of Szilard’s classical single-particle engine, we modeled the Szilard engine as a quantum thermodynamical system—an information engine consisting of a simple thermodynamic system that interacts with quantum control system (quantum demon). Taking Szilard’s original strategy to heart the analyzes the physics of both the thermodynamic system and control system. In agreement with Szilard, over the entire thermodynamic cycle the net changes (uptake or exhausting of resources) balance each other out. There is zero output work and the operation is consistent with the Second Law. In particular, as Ref. [38] establishes:

$$\begin{aligned} \Delta U^I + \Delta U^C &= 0 \\ \Delta U^M + \Delta U^E &= 0, \end{aligned}$$

and

$$\begin{aligned} \Delta Q^I + \Delta Q^C &= -(\Delta Q^M + \Delta Q^E), \\ W^I + W^C &= -(W^M + W^E). \end{aligned}$$

That said, portions of the engine’s cycle exhibit interesting behavior and trade-offs. In particular, they show a nontrivial relationship to Landauer’s Principle. Specifically, while the QSE violates Landauer’s Principle, the aggregate entropic cost of measurement and erasure still satisfies it:

$$\langle Q_{erasure} \rangle + \langle Q_{measurement} \rangle \leq k_B T H(\delta),$$

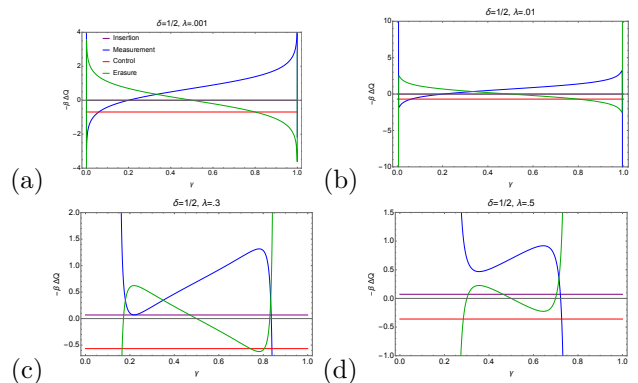


FIG. 9. Thermodynamic costs $\Delta Q/k_B T$ vs γ in semiclassical limit for measurements (blue dash line), control (red dotted line), and erasure (green solid line). Partition $\delta = 1/2$. (a) $\lambda_D = 0.001$. (b) $\lambda_D = 0.01$. (c) $\lambda_D = 0.3$. (d) $\lambda_D = 0.5$.

as Refs. [41–44] previously noted for the classical engine.

This highlights interesting trade-offs between the entropic costs of erasure and measurement. Their nature was explored by examining the detailed thermodynamic costs of each engine stage; see Figs. 5, 6, and 7 and the costs functional dependence on δ and γ . In particular, the emergence of nonmonotonic behavior of the entropic cost as a function of $|\delta - 0.5|$, and its lack of (left/right) symmetry with respect to $\delta \rightarrow 1 - \delta$ transformation is due to the lack of symmetry between the demon’s informational states for an arbitrary value $\gamma \neq 0.5$.

While the Second Law is not violated—all entropic contributions sum to zero, Fig. 9—the thermodynamic signature of the individual stages varies significantly. Thus, these thermodynamic trade-offs are key to designing quantum engines. For example, at $\delta = \gamma = 1/2$, the entropic cost of erasure vanishes, violating Landauer’s Principle. However, it still respects the trade-off thanks to the fact that $\langle Q_{measurement} \rangle = \log 2$.

Conclusion. We revisited Szilard’s engine from the broader perspective of a quantum information engine—a quantum machine that manipulates both energy and information to produce work and dissipate heat. Including the controller (demon), and its quantum nature, into the engine’s description allowed us to explore a variety of nonclassical thermodynamic behaviors that, while being compatible with the principles of quantum thermodynamics, exhibited new and different thermodynamic signatures. This method of analyzing controlled quantum systems can be generalized to arbitrary quantum information engines and so will be of interest to designing efficient quantum information processing devices.

Acknowledgments F.A. and J.P.C. thank the Telluride Science Research Center for its hospitality during visits. This material is based on work supported by, or in part

by, a Templeton World Charity Foundation Power of Information Fellowship, Foundational Questions Institute

Grant FQXi-RFP-IPW-1902, and U.S. Army Research Laboratory and the U. S. Army Research Office under contracts W911NF-13-1-0390 and W911NF-18-1-0028.

-
- [1] J. C. Maxwell. *Theory of Heat*. Longmans, Green and Co., London, United Kingdom, ninth edition, 1888. 1
- [2] J. A. Wheeler. The computer and the universe. *Intl. J. Theo. Phys.*, 21(6/7):557–572, 1982. 1
- [3] J. A. Wheeler. Information, physics, quantum: The search for links. In W. Zurek, editor, *Entropy, Complexity, and the Physics of Information*, volume VIII of *SFI Studies in the Sciences of Complexity*, Reading, Massachusetts, 1990. Addison-Wesley.
- [4] R. Landauer. Information is physical. *Physics Today*, pages 23–29, May 1991. 1
- [5] L. Szilard. On the decrease of entropy in a thermodynamic system by the intervention of intelligent beings. *Z. Phys.*, 53:840–856, 1929. 1
- [6] R. Landauer. Energy requirements in communication. *App. Phys. Lett.*, 51(24):551–562, 1987. 1
- [7] C. H. Bennett. Thermodynamics of computation—A review. *Intl. J. Theo. Phys.*, 21(3-4):905, 1982. 1
- [8] H. Leff and A. Rex. *Maxwell’s Demon 2: Entropy, Classical and Quantum Information, Computing*. Taylor and Francis, New York, 2002. 1
- [9] U. Seifert. Stochastic thermodynamics, fluctuation theorems and molecular machines. *Rep. Prog. Phys.*, 75:126001, 2012. 1
- [10] J. M. R. Parrondo, J. M. Horowitz, and T. Sagawa. Thermodynamics of information. *Nature Physics*, 11:131–139, 2015. 1
- [11] A. B. Boyd and J. P. Crutchfield. Maxwell demon dynamics: Deterministic chaos, the Szilard map, and the intelligence of thermodynamic systems. *Phys. Rev. Lett.*, 116:190601, 2016. 1, 2, 5
- [12] A. B. Boyd, D. Mandal, and J. P. Crutchfield. Identifying functional thermodynamics in autonomous Maxwellian ratchets. *New J. Physics*, 18:023049, 2016. 1
- [13] M. Hamed Mohammady and J. Anders. A quantum Szilard engine without heat from a thermal reservoir. *New J. Phys.*, 2017. 1
- [14] W. Zurek. Eliminating ensembles from equilibrium statistical physics: Maxwell’s demon, Szilard’s engine, and thermodynamics via entanglement. *Phys. Rep.*, 755:1–21, 2018. 3
- [15] R. Alicki and M. Horodecki. Information-thermodynamics link revisited. *J. Phys. A: Math. Theor.*, 2019.
- [16] T. Sagawa and M. Ueda. Minimal energy cost for thermodynamic information processing: measurement and information erasure. *Phys. Rev. Lett.*, 102(25):250602, 2009.
- [17] H. Li, J. Zou, J.-G. Li, B. Shao, and L.-A. Wu. Revisiting the quantum Szilard engine with fully quantum considerations. *Annals of Physics*, 327(12):2955–2971, 2012.
- [18] A. Aydin, A. Sisman, and R. Kosloff. Landauer’s principle in a quantum Szilard engine without Maxwell’s demon. *Entropy*, 22(3):294, 2020.
- [19] S. W. Kim, T. Sagawa, S. De Liberato, and M. Ueda. Quantum Szilard engine. *Phys. Rev. Lett.*, 106(7):070401, 2011.
- [20] C. Y. Cai, H. Dong, C. P. Sun, et al. Multiparticle quantum Szilard engine with optimal cycles assisted by a Maxwell’s demon. *Phys. Rev. E*, 85(3):031114, 2012.
- [21] H. J. Jeon and S. W. Kim. Optimal work of the quantum Szilard engine under isothermal processes with inevitable irreversibility. *New J. Physics*, 18(4):043002, 2016.
- [22] J. Bengtsson, M. N. Tengstrand, A. Wacker, P. Samuelsson, M. Ueda, H. Linke, and S. M. Reimann. Quantum Szilard engine with attractively interacting bosons. *Phys. Rev. Lett.*, 120(10):100601, 2018.
- [23] J. Song, S. Still, R. D. H. Rojas, I. P. Castillo, and M. Marsili. Optimal work extraction and mutual information in a generalized Szilard engine. *arXiv preprint arXiv:1910.04191*, 2019.
- [24] Z. Zhuang and S.-D. Liang. Quantum Szilard engines with arbitrary spin. *Phys. Rev. E*, 90(5):052117, 2014.
- [25] Y. Lu and G. L. Long. Parity effect and phase transitions in quantum Szilard engines. *Phys. Rev. E*, 85(1):011125, 2012.
- [26] K.-H. Kim and S. W. Kim. Szilard’s information heat engines in the deep quantum regime. *J. Korean Physical Soc.*, 61(8):1187–1193, 2012.
- [27] J. Bengtsson, M. N. Tengstrand, and S. M. Reimann. Bosonic Szilard engine assisted by Feshbach resonances. *Phys. Rev. A*, 97(6):062128, 2018.
- [28] H. Dong, D. Z. Xu, C. Y. Cai, C. P. Sun, et al. Quantum Maxwell’s demon in thermodynamic cycles. *Physical Review E*, 83(6):061108, 2011. 1
- [29] J. V. Koski, V. F. Maisi, and J. P. Pekola. Experimental realization of a Szilard engine with a single electron. *Proc. Natl. Acad. Sci. USA*, 111(38):13786–13789, 2014. 1
- [30] P. A. Camati, J. P. S. Peterson, T. B. Batalhao, K. Micaeli, A. M. Souza, R. S. Sarthour, I. S. Oliveira, and R. M. Serra. Experimental rectification of entropy production by Maxwell’s demon in a quantum system. *Phys. Rev. Lett.*, 117(24):240502, 2016.
- [31] W-B Wang, X-Y Chang, F Wang, P-Y Hou, Y-Y Huang, W-G Zhang, X-L Ouyang, X-Z Huang, Z-Y Zhang, H-Y Wang, et al. Realization of quantum Maxwell’s demon with solid-state spins. *Chinese Phys. Lett.*, 35(4):040301, 2018.
- [32] J. P. S. Peterson, R. S. Sarthour, and R. Laflamme. Implementation of a quantum engine fueled by information. *arXiv:2006.10136*, 2020.

- [33] M. D. Vidrighin, O. Dahlsten, M. Barbieri, M. S. Kim, V. Vedral, and I. A. Walmsley. Photonic Maxwell's demon. *Phys. Rev. Lett.*, 116(5):050401, 2016.
- [34] N. Cottet, S. Jezouin, L. Bretheau, P. Campagne-Ibarcq, Q. Ficheux, J. Anders, A. Auffeves, R. Azouit, P. Rouchon, and B. Huard. Observing a quantum Maxwell demon at work. *Proc. Natl. Acad. Sci.*, 114:7561, 2017.
- [35] M. Naghiloo, J. J. Alonso, A. Romito, E. Lutz, and K. W. Murch. Information gain and loss for a quantum Maxwell's demon. *Phys. Rev. Lett.*, 121:030604, 2018. 1
- [36] R. Landauer. Irreversibility and heat generation in the computing process. *IBM J. Res. Develop.*, 5(3):183–191, 1961. 1, 4
- [37] M. A. Nielsen and I. L. Chuang. *Quantum Computation and Quantum Information*. Cambridge University Press, Cambridge, United Kingdom, tenth anniversary edition, 2011. 2
- [38] M. Ashrafi, F. Anza, and J. P. Crutchfield. The quantum Szilard engine. *arXiv:2012:XXXXX*, 2020. 2, 3, 4, 5
- [39] Y. N. Joklegar. Particle in a box with a δ -function potential: Strong and weak coupling limits. *Am. J. Phys.*, 2009. 3
- [40] P. Pedram. Exact solutions of a particle in a box with a delta function potential: The factorization method. *Am. J. Phys.*, 2010. 3
- [41] K. Shizume. Heat generation required by information erasure. *Phys. Rev. E*, 52(4):3495–3499, 1995. 5
- [42] F. N. Fahn. Maxwell's demon and the entropy cost of information. *Found. Physics*, 26:71–93, 1996.
- [43] M. M. Barkeshli. Dissipationless information erasure and Landauer's principle. *arXiv:cond-mat*, page 0504323, 2006.
- [44] T. Sagawa. Thermodynamics of information processing in small systems. *Prog. Theo. Phys.*, 127(1):1–56, 2012. 5